




Investigation of Cr addition effect on structural, morphological, electrical and magnetic properties of Bi(Pb)-2212 superconductors

S. Menassel^{1,*} , A. Galluzzi^{2,5}, Y. Boudjadja³, S. P. Altintas⁴, C. Terzioglu⁴, and M. Polichetti^{4,5}

¹ Faculty of Science and Technology, Mohamed Boudiaf University, 28000 Msila, Algeria

² Department of physics "E.R. Caianiello", Salerno University, Via Giovanni Paolo II 132, Fisciano, 84084 Salerno, Italy

³ LEND, Faculty of science and technology, Jijel University, Bp 98 Ouled Aissa, 18034 Jijel, Algeria

⁴ Department of Physics, Abant Izzet Baysal University, 14280 Bolu, Turkey

⁵ CNR-SPIN Salerno, Via Giovanni Paolo II 132, Fisciano, 84084 Salerno, Italy

Received: 12 November 2022

Accepted: 21 April 2023

Published online:

15 May 2023

© The Author(s), under exclusive licence to Springer Science+Business Media, LLC, part of Springer Nature 2023

ABSTRACT

The main purpose of this research work will assess the effect of Cr addition on the properties of $\text{Bi}_{1.8}\text{Pb}_{0.4}\text{Sr}_2\text{CaCu}_2\text{O}_{8+d}$ superconducting ceramics. The samples are produced from industrial powders with different amounts of Cr (0, 1, 2, 3, 4, 5, 6 and 7 wt %) by sol–gel synthesis route. The influence of doping element has been determined by X-ray diffraction (XRD), scanning electron microscopy (SEM), electrical resistivity and magnetic characterizations. In particular, the eventual presence of secondary phases as a result of Cr doping on the undoped sample was investigated by using XRD. By means of SEM analysis, the Cr doping influence on the grain morphology of the samples was explored. Contrarily, the $T_{c,on}$ and the $T_{c,off}$ of the samples have been obtained by using electrical resistivity measurements and their behavior as a function of the Cr doping has been discussed. Finally, by performing magnetization analysis versus temperature and magnetic field, the behavior of the critical temperature T_c and of the critical current density J_c as a proportion of the Cr concentration has been discussed.

1 Introduction

Since their discovery, high-temperature superconductors have been classified as future materials, including those based on bismuth with higher critical density and irreversible field. These characteristics have favored these materials in various applications,

such as medical diagnostics, high-speed trains (magnetic levitation), high-power transmission lines, energy storage systems, etc." [1, 2].

From the literature of high-temperature superconductors (HTSC) [3], a numerous research works were to comprehend the characteristics of this kind of materials. Many researches are performed for the

Address correspondence to E-mail: sihem_menassel@yahoo.fr; sihem.menassel@univ-msila.dz

Bi(Pb)–Sr–Ca–Cu–O system (BSCCO) in order to increasing their critical current density J_c for practical field. However, these materials are sensitive to magnetic field, the critical current in the plans a-b decreases rapidly when the magnetic field increases. In this case the decreasing is more rapid whenever the field lines up with the c axis of the grains. Indeed, the low number of defects in the plans [CuO₂] facilitates the movement of vortices under the effect of a Lorentz force. Until the magnetic field is perpendicular to the c axis, the vortices are anchored between the [CuO₂] planes. The critical current therefore decreases more slowly with the magnetic field. This decrease is even slower when the ceramic grains are correctly oriented. It was confirmed that the BSCCO composites are appropriate for various transport applications once handled appropriately to achieve a satisfactory grain alignment [4–6]. Furthermore, it is pretty apparent that BSCCO superconductors have the highest values in critical current densities, critical transition temperatures (T_c), and irreversibility fields. These compounds achieved be alloys or transition metals with high electrical resistance values in the normal state, they contain flat layers of copper and oxygen atoms. These copper oxide layers carry the supercurrent, give a high T_c value, and it demonstrates greater stability in superconductors properties. The general chemical formula for Bi-based HTSC could become given by $\text{Bi}_2\text{Sr}_2\text{Ca}_{n-1}\text{Cu}_2\text{O}_{2n+4}$. (Where $n = 1, 2$ and 3 which n represent the number of CuO_2 layers and transition temperatures are 20, 95 and 110 K, respectively) [7]. The Bi-2212 component is considered a superconductor composite with more possibility to be employed in technology [8–12].

The chemical doping of HTSC is controllable, effective method for enhancing the mechanic, morphological and superconductivity properties of these materials.

Many chemical rare earth elements have been playing a significant effect on the nanostructure, electrical and magnetization characteristic of the superconducting materials [13–18]. The influence of excessive-doping and under-doping on T_c zero has been tested, in this regard substitutions and addition of doped element lead to stabilize the Bi-2212 phase where it exhibits the best superconducting behavior. Recently superconductivity has been discovered in chromium based compounds (CrAs, 2.2 K) with moderate magnetic moment. For this reason we have chosen Cr as dopant for the structural and magnetic

properties of our superconducting material Bi2212. Moreover, Chromium metal discovered by L. N. Vauquelin in 1797 is another interesting rare earth element with exceptional magnetic properties. at room temperature, it is the only elemental solid to exhibit anti-ferromagnetic ordering. It is a transition metal, within atomic radius (140 pm) and electrical resistivity about 125 NΩ.m. Also, with the replacement of Pb in Bi increase the critical current densities [8, 19–23], and reduces the lattice parameter c , It influences the extra oxygen absorbed from the BiO layers. then reduces the anisotropic behavior of superconducting proprieties.

Besides chemical doping, the method and synthesis conditions must be chosen carefully. Unlike the sol-gel method, wet-chemistry synthesis techniques [24–32], including, solid state reaction, co-precipitation method, citrate gel process, oxidation of liquid quenched precursor alloys, and matrix reaction. Almost all of those methods have difficulties and limits that come with the actual process and the performance of the material it produces.

Sol-gel is one of the most preferred methods due to colloid solution combustion synthesis, the process synthesis on high-purity multi component, and a low temperature initiated combustion process that is found to be cost-effective for the preparation of extremely fine and homogeneous powders.

For the advancement in this area of study, Our work discusses the effect of Cr on the morphological and magnetic characteristics of Bi(Pb)-2212 composites synthesized by the sol-gel process.

2 Experimental details

2.1 Chemical synthesis

In stoichiometric proportions, $\text{Bi}(\text{NO}_3)_3$, $\text{Pb}(\text{NO}_3)_2$, $\text{Sr}(\text{NO}_3)_2$, $\text{Ca}(\text{NO}_3)_2$ and $\text{Cu}(\text{NO}_3)_2$ are dissolved in distilled water.

Bi solution is amended with Cr_2O_3 powder dissolved in nitric acid.

$\text{Bi}_{1.8}\text{Pb}_{0.4}\text{Sr}_2\text{CaCu}_2\text{Cr}_x\text{O}_8 + d$, where $x = 0, 1, 2, 3, 4, 5, 6,$ and 7 wt%, is the nominal composition of the prepared samples. They will be labeled accordingly as Cr0, Cr1, Cr2, Cr3, Cr4, Cr5, Cr6, and Cr7.

The solution of ammonia reacts with citric acid to produce a triammonium citrate with a 2 mol/kg content.

Acrylamide $\text{CH}_2=\text{CHCONH}_2$ and N, N methylene diacrylamide $\text{CH}_2=\text{CHCONHCH}_2\text{NHCOCH}=\text{CH}_2$ are combined to make organic gels and complex the Bi, Ca, Sr, and Cu cations. On a hot plate, the resulting solution is mixed, stirred, and heated to 80°–90 °C with a magnetic stirrer. Some drops of an AIBN solution (2,2'-azobis(2-methylpropionitrile). in acetone are added to speed up the gel's formation. This material is converted to Bi(Pb)-2212 by thermal treatment at 400 °C for two hours and 700 °C for six hours, respectively. In agate mortar, the powder is ground and then calcined for 12 h at 860 °C, reaching a speed of 5 °C/min.

2.2 Measurements

To perform phase analysis on the materials, X-ray diffraction (XRD) is used on a Siemens D8-Advance powder diffractometer by applying the application of CuK radiation ($\lambda = 1.5418 \text{ \AA}$) with an angle increment of 0.02 in the range $2\theta = 10\text{--}55^\circ$. The samples' microstructure and surface morphology are of examined by scanning electron microscopy (SEM, JEOL 6390LV) equipped with an energy dispersive. All samples are tested for resistivity between 10 and 120 K using a typical DC four-probe method with a current of 5 mA on helium refrigerator operating in a closed cycle (Cryodine CTI-Cryogenics). The current connections and voltage are created using a silver paste in which the magnetic field is used parallel to the pellet's surface and perpendicular to the current's direction of flow.

Magnetization measurements were taken as a function of temperature $m(T)$ and field $m(H)$ utilizing a QD-PPMS equipment with a VSM option [33] It has been paid attention to reduce the residual entrapped field inside the superconducting magnet before each measurement [34, 35]. The sample was cooled in zero field to make the $m(T)$ measurement. Then the magnetic field is activated and data acquired while increasing the temperature. After that, the sample has been cooled down again but this time in presence of field. This procedure allows to record data in Zero Field Cooling (ZFC) and Field Cooling (FC) conditions [36, 37], respectively. The $m(H)$ measurement was obtained by first cooling the sample to 4.2 K in zero field, then ramping the field from 0 T to + 9 T, then -9 T, and finally back to + 9 T [38, 39].

The samples were examined in a dc magnetic field that was directed perpendicular to the sample's

biggest face. The magnetic moment in relationship to temperature ($m(T)$), values has been calculated under Zero Field Cooling (ZFC)-Field Cooling (FC) conditions to determine a superconducting critical temperature T_c of our sample.

Precisely, the sample is cooled to 40 K without a magnetic field; then, the magnetic field is turned on at 0.002 T, and data are collected for temperature increase (ZFC) up to 100 K.

The sample is then cooled again, and the FC magnetic moment is obtained in the presence of a field.

3 Results and discussion

3.1 X-ray diffraction analysis

Figure 1a shows XRD pattern of the Bi(Pb)-2212 composites prepared with different contents of Cr. In addition to the lines of the main phase, (+)-marked extra tiny lines are observed.

According to the JCPDS46-0392 file, they correspond to the Bi-2201 phase with a low T_c .

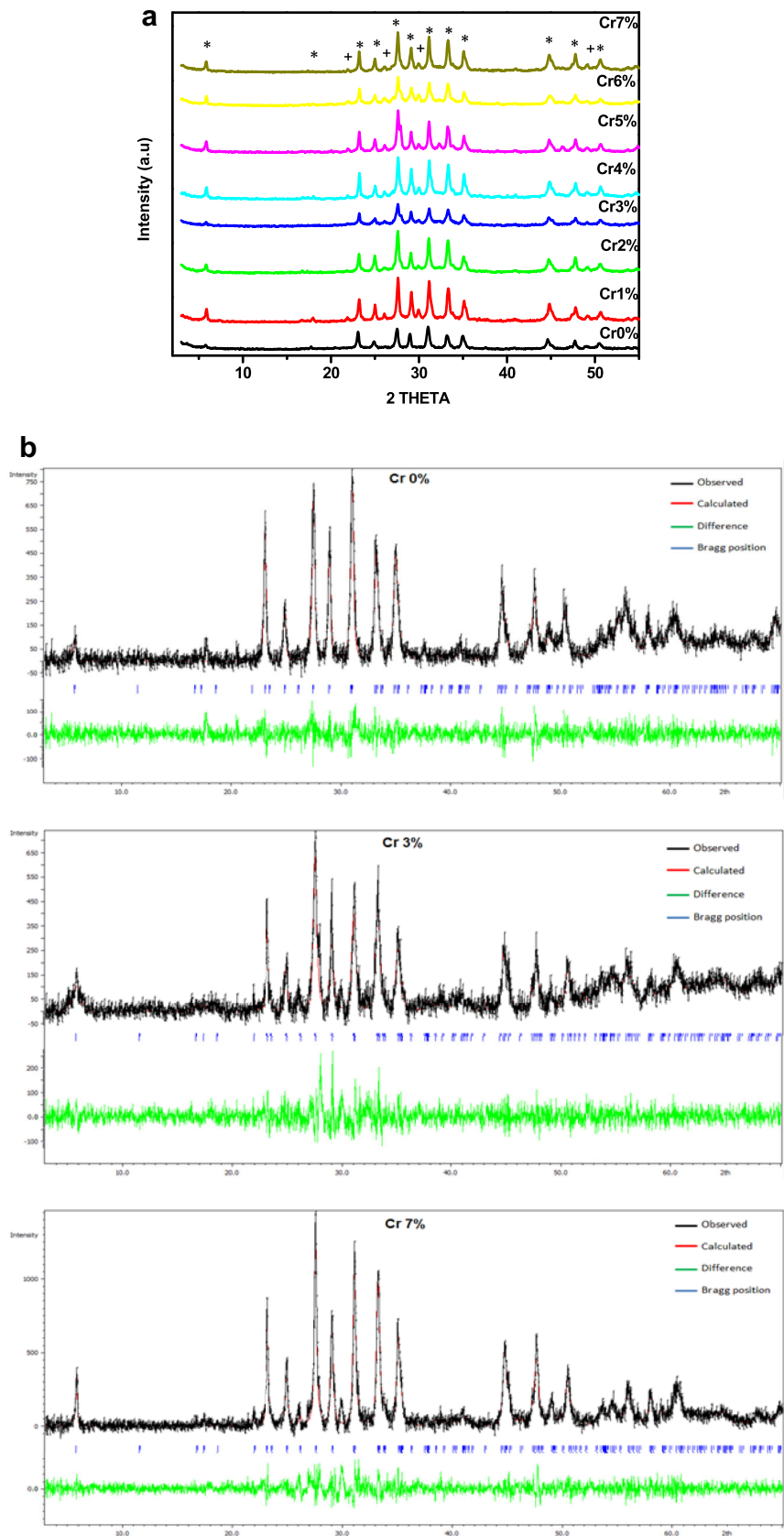
The addition of Cr affects the intensity of the peaks and the appearance of secondary peaks when the amount of Cr is increased, indicating that Cr^{3+} ions are incorporated into the matrix. This result corresponds to the Cr solubility limit in Bi(Pb)-2212.

The cell characteristics are refined using the JANA 2006 program [40] and the Bbmb space group [41]. The line intensities are fitting by a pseudo-Voigt functional, the backdrop is described by 36 terms of Legendre polynomials, and the asymmetric is corrected using the Berar-Baldinazzi method.

Figure 1b shows XRD data of three samples, 0%, 3% and 7% analyzed by Rietveld refinement method. This method is based on the construction of diffraction patterns calculated according to a structural model [42]. The background was corrected using a Legendre polynomials. A peak profile function was modeled using a convolution of the pseudo-Voigt function with the asymmetry function described by Berar-Baldinazzi correction.

Table 1 presents the obtained parameters synthesized by modified sol-gel method. When there is an increase in chromium concentration, there is typically a decreasing trend in the parameters c . These behaviors can be interpreted by substitution of Cu-ion by Cr-ion in the structure, which reduces the

Fig. 1 **a** XRD patterns of the nonadded and Cr₂O₃ added Bi_{1.8}Pb_{0.4}Sr₂CaCuO₈ + d tapes. peaks according to the Bi-2212 and Bi-2201 phases are marked by * and +, respectively. **b** Rietveld refinement for Cr 0%, Cr 3% and Cr 7% samples



oxygen levels in the unit cell [43, 44]. As seen from the graph no secondary phase Bi2201 appears in undoped sample, however it begins to rise as the Cr addition is increased.

By applying the appropriate standard modeling approach [45], the relative volume fractions (Table 1) of the Bi-2212 and Bi-2201 phases in each sample are determined from the intensities of the reflections:

$$X_{\text{phase}i} = \frac{\sum I_{\text{phase}i}(\text{peaks})}{\sum I_{2212}(\text{peaks}) + \sum I_{2201}(\text{peaks})} \tag{1}$$

Phase $i = \text{Bi-2212 or Bi-2201}$, where I_{2212} and I_{2201} are the XRD intensities of Bi-2212 and Bi-2201 phases, respectively. It can be clearly seen in Table 1 that the Bi-2201 secondary phase is more evident in doped samples and the addition of Cr decreases the intensities of Bi-2212 and increases the intensities of Bi-2201. The undoped sample has higher volume fraction of the Bi-2212 phase (90%) than other samples.

The average crystallite size (D) has calculated from Debye–Scherrer formula [46]:

$$D = \frac{0.9\lambda}{\beta \cos\theta}, \tag{2}$$

where λ is the wavelength, β is the full width at half maximum FWHM and θ is the angle of the intense peak. From Table 2 the crystallite size decrease with the increase of Cr addition.

3.2 SEM results

The contribution of Cr doping on the morphological characteristics of $\text{Bi}_{1.8}\text{Pb}_{0.4}\text{Sr}_2\text{CaCu}_2\text{Cr}_x\text{O}_{8+d}$ ceramics is studied in more detail with scanning electron microscopy, which is used to capture image of certain areas as microanalysis. Figure 2 has shown the SEM micrographs of the pure and Cr-addition samples

taken at the same magnification (5000X) with a size of about 2 μm from the surface of the pellets. Doping with Cr doesn't seem to have much of an effect on the morphology of the grain. It's easy to see that the shape of the grains in all of all samples is very similar. The characteristic flaky grains of Bi-2212 are visible. However, it is observed that the undoped sample is denser, contain small sized grains with connectivity. This fact could induce better transport superconducting properties. So, doping with Cr worsens the surface morphology.

The addition of Chrom in the grains of the doped samples was confirmed by qualitative EDX analysis presented in the Fig. 2. Our spectrum shows the absence of the parasite phases in all samples.

3.3 DC electrical resistivity measurements

The electrical resistivity versus temperature $\rho(T)$ of the samples, calculated using the standard four-probe dc technique between 40 and 110 K, is displayed in Fig. 3. The above data are normalized to the resistivity ρ_n at 110 K. All samples display a metallic-like character in the normal state. It can be easily seen that both $T_{c,on}$ and $T_{c,off}$ changes with doping. The values of parameters like $T_{c,on}$, $T_{c,off}$ and superconducting transition width ΔT_c for different amounts of Cr are listed in Table 3. Possible causes for a difference in T_c include the induction of mobile carriers, the total oxygen concentration, and the disorder in the CuO_2 planes.

All samples have an almost identically narrow width of transition temperature, suggesting that there is just one superconductivity transition. Contrarily, larger transition widths are sometimes associated with a high disoriented angle, hence reducing intergranular connectivity. [47].

Table 1 Samples parameters and resistivity measurement results for $\text{Bi}_{1.8}\text{Pb}_{0.4}\text{Sr}_2\text{CaCu}_2\text{Cr}_x\text{O}_{8+d}$

Samples	$T_{c, on}(K)$	$T_{c, off}(K)$	$\Delta T(K)$	$c (\text{\AA})$	Volume fraction (%)		Hole concentration (P)
					2212	2201	
Cr0%	78.70	72.79	5.91	30.80	90	10	0.431
Cr1%	83.87	73.10	10.77	30.72	76	24	0.420
Cr2%	85.26	73.37	11.89	30.72	73	27	0.429
Cr3%	86.48	68.71	17.77	30.68	71	28	0.417
Cr4%	78.96	55.25	23.71	30.66	71	29	0.414
Cr5%	81.37	66.05	15.32	30.66	71	29	0.411
Cr6%	87.02	64	22.14	30.66	70	30	0.416
Cr7%	86.43	65.73	20.7	30.65	70	30	0.418

Table 2 Unit cell parameters, crystallite size for each of the samples

	Cr0%	Cr1%	Cr2%	Cr3%	Cr4%	Cr5%	Cr6%	Cr7%
<i>a</i> (Å)	5.3782	5.3785	5.3746	5.3927	5.3661	5.3646	5.3670	5.3750
<i>c</i> (Å)	30.8026	30.7225	30.7209	30.6858	30.6683	30.6669	30.6571	30.6941
2θ (°)	31.041	31.161	31.161	31.162	31.160	31.105	31.041	31.193
D (nm)	25.98	25.53	23.89	23.79	23.42	21.94	21.11	20.53

Hole-carrier concentrations p per Cu-ion are estimated for each sample using the Eq. (3), [7]:

$$P = 0.16 + \left[\left(1 - \frac{T_{c,on}}{T_{c,max}} \right) / 82.6 \right]^{1/2} \quad (3)$$

while $T_{c,max}$ has been assumed to be 95 K for Bi-2212 phase [26] and $T_{c,off}$ values were derived in Table 1.

Doping modifies the behavior of the sample from an overdoped zone to an appropriately doped region.

The minimal hole number of 0.417 observed for the Cr3% amount indicates that it is closest to an optimal manner doped area.

Therefore, the inclusion of trivalent Cr3 + reduces the number of efficient holes.

The $T_{c,on}$ of all samples correlates better with the holes 's concentration of CuO2 layers.

3.4 Magnetic results

All the measured curves are reported in the left panel of Fig. 4. The temperature value associated with the onset of the ZFC magnetic moment drop is defined as the T_c , and its behavior as a function of Chrome doping is reported in Table 3 and in the right panel of Fig. 4. It is visible how, starting from the undoped sample, the T_c value increases up to 4% Cr doping concentration [48]. Further increasing the doping percentage, the T_c starts to decrease. This dome shape-like behavior is usually attributed to an increase in the carrier density due to the doping. In fact, an under/optimal-doping causes a pressure induced charge transfer which enhances the T_c value in the HTSC while an over-doping determines an increase in coulomb correlation which causes a lowering of T_c values [49, 50].

In Fig. 5, the $m(H)$ curves for various samples have been presented. The existence of flux pinning centers is visible looking at the $m(H)$ shape [51]. Moreover, possibly surface barriers are present when the superconducting hysteresis loops are not

symmetrical [52]. Understanding how the Cr doping effects on the transport capabilities of the sample, the Bean critical state approach has been applied to determine the critical current density J_c from $m(H)$ curves [53–55] Since J_c is dependent on the width of the hysteresis loop, the formula (4) for calculating it in slab geometry is as follows:

$$J_c = \frac{20\Delta M}{[b(1 - \frac{b}{3a})]}, \quad (4)$$

where $\Delta M = M_{dn} - M_{up}$, M_{dn} and M_{up} refers for magnetization, which can be measured with decreasing and increasing applied field, accordingly, a (cm) and b (cm) are the sample dimensions ($b < a$).

It is evident that the general shape of J_c is typical for type-II superconductors (Fig. 6, left panel) without the presence of peculiar phenomena such as second magnetization peak effect or multidomain J_c behavior [56–59] very often due to pinning crossover and/or vortex dynamics which can be efficiently studied by using the multiharmonic ac magnetic susceptibility method [60–62]. By extracting the value of J_c at fixed fields from the $J_c(-H)$ curves reported in the left panel of Fig. 6, the J_c can be plotted as a function of the Cr doping concentration for various magnetic fields (see right panel of Fig. 6). In this graph it is visible how the J_c drops at 1% Cr doping for all the fields. Then, increasing the Cr doping to 2%, the J_c starts to increase for all the fields until it reaches its maximum value for a Cr doping concentration equal to 3% for all the fields. This development is a result of the decrease in intrinsic anisotropy and to the fact that the addition can provide new efficient pinning centers at highest fields [45]. On the other hand, for higher amount of Cr, the J_c values start to decrease probably due to an excessive number of impurities which locally destroys the superconductivity phase of the sample so worsening its current transport capabilities.

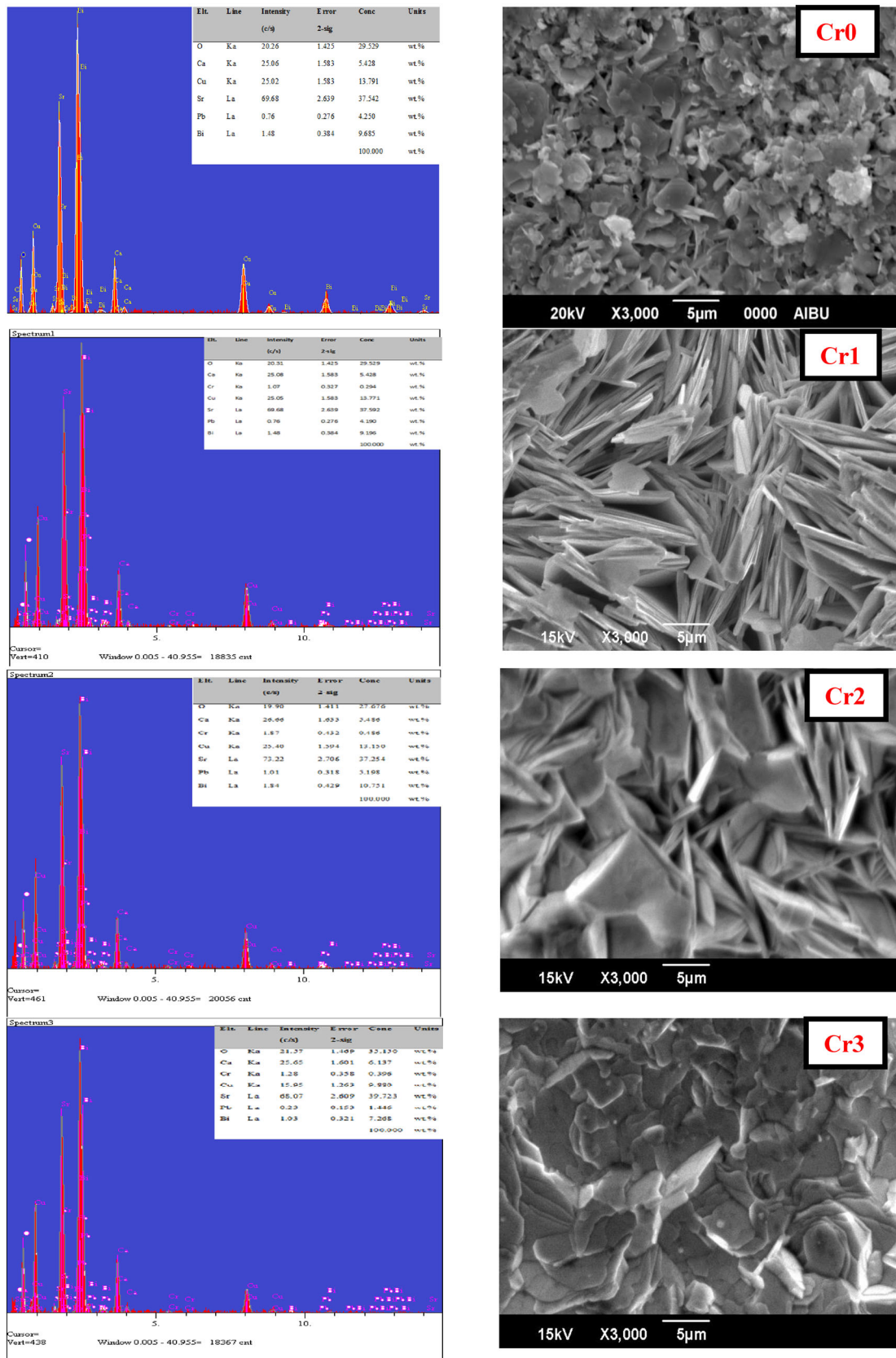


Fig. 2 SEM micrographs of added and nonadded samples. In the right panel EDS spectrums of samples with chemical composition

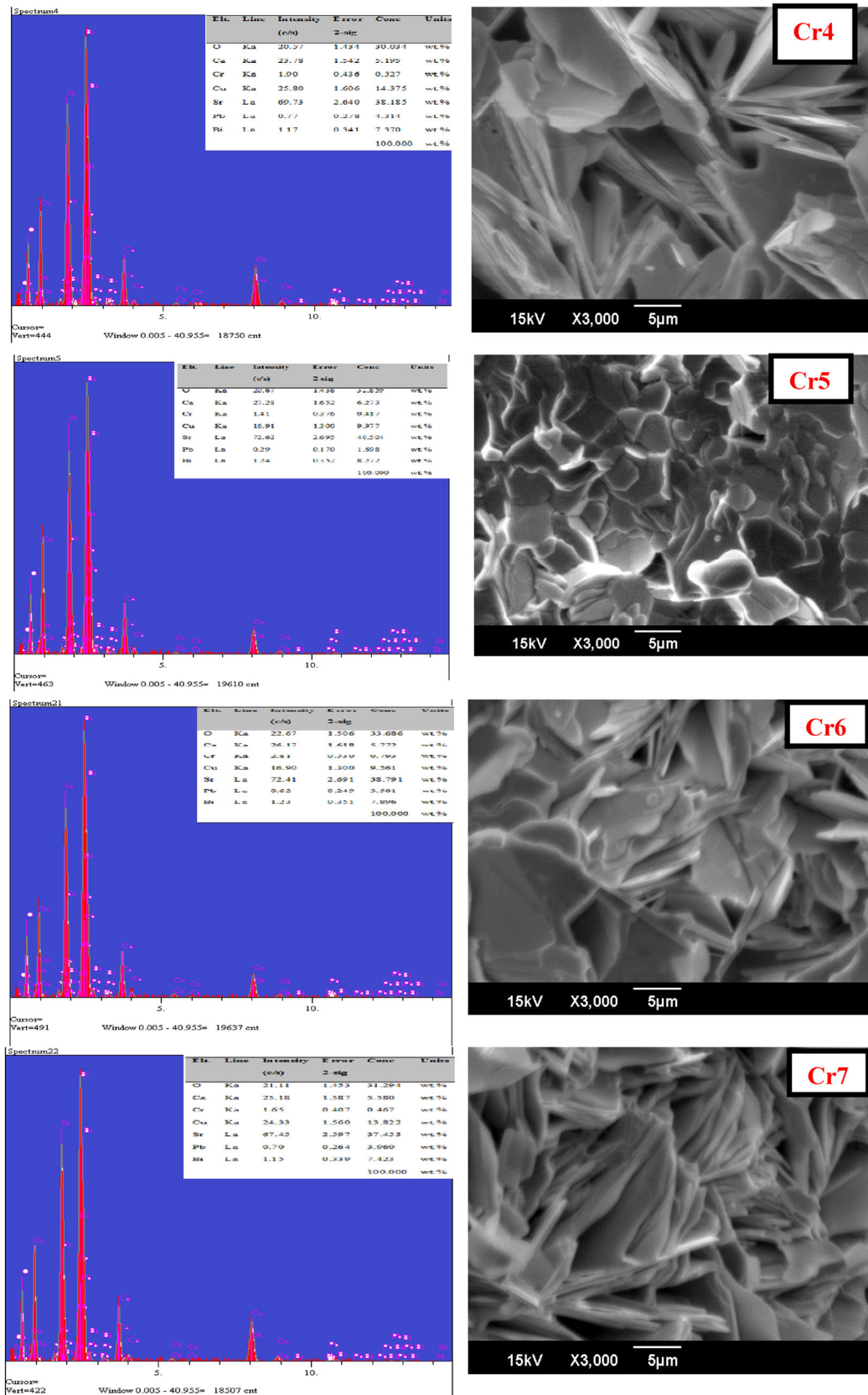


Fig. 2 continued

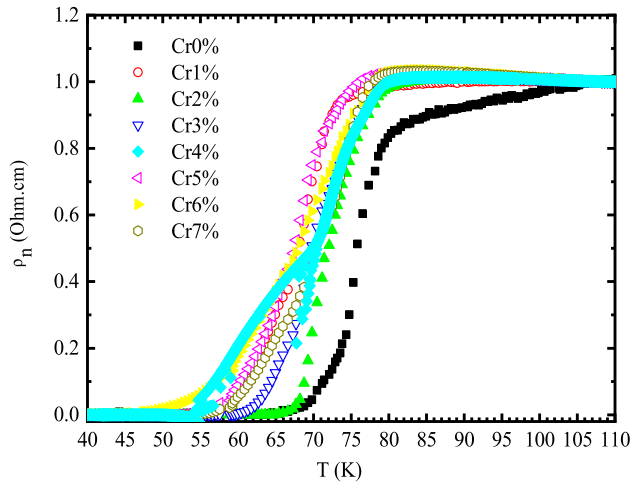


Fig. 3 Electrical resistivity versus temperature curves for $\text{Bi}_{1.8}\text{Pb}_{0.4}\text{Sr}_2\text{CaCu}_2\text{Cr}_x\text{O}_{8+d}$

Table 3 Superconducting critical temperatures for $\text{Bi}_{1.8}\text{Pb}_{0.4}\text{Sr}_2\text{CaCu}_2\text{Cr}_x\text{O}_{8+d}$ extracted from the $m(T)$ curves

Sample	T_c (K)
Pure	76 ± 0.2
Dop1% Chrome	$81,3 \pm 0.2$
Dop2% Chrome	$83,5 \pm 0.2$
Dop3% Chrome	84 ± 0.2
Dop4% Chrome	$84,4 \pm 0.2$
Dop5% Chrome	$82,8 \pm 0.2$
Dop6% Chrome	$82,4 \pm 0.2$
Dop7% Chrome	$82,3 \pm 0.2$

4 Conclusion

X-ray diffraction (XRD), scanning electron microscopy (SEM), electrical resistivity, and magnetic characterizations were performed on various $\text{Bi}_{1.8}\text{Pb}_{0.4}\text{Sr}_2\text{CaCu}_2\text{Cr}_x\text{O}_8 + d$ samples with $x = 0, 1, 2, 3, 4, 5, 6,$ and 7 wt%.

We discovered other smaller lines attributable to the Bi-2201 low T_c phase appearing in the doped samples using X-ray diffraction analysis, in addition to the main 2212 phase lines.

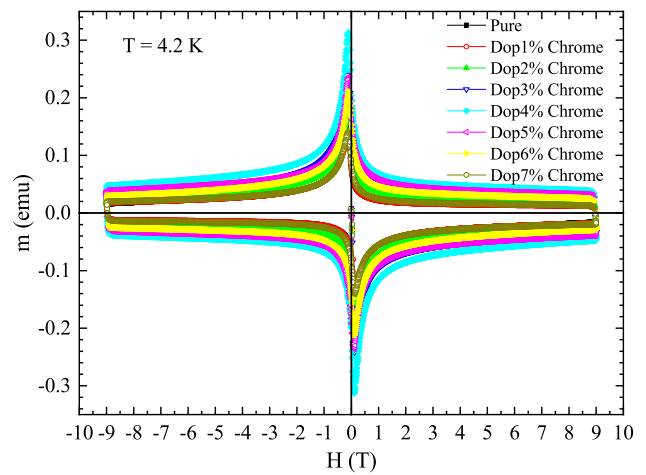


Fig. 5 Superconducting hysteresis loops for $\text{Bi}_{1.8}\text{Pb}_{0.4}\text{Sr}_2\text{CaCu}_2\text{Cr}_x\text{O}_{8+d}$

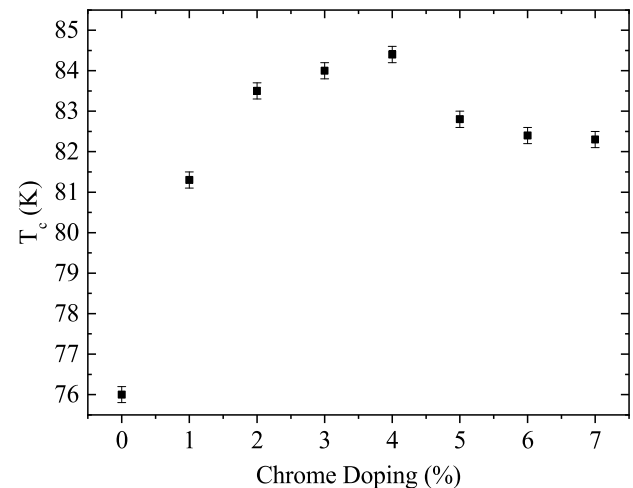
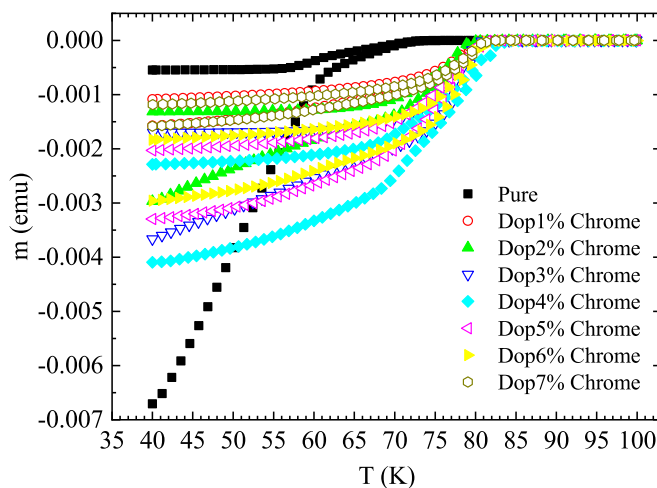


Fig. 4 Magnetic moment as a function of temperature $m(T)$ measured in ZFC–FC conditions with an applied magnetic field of 0.002 T (left). In the right panel the superconducting critical temperature is plotted as function of the Chrome doping

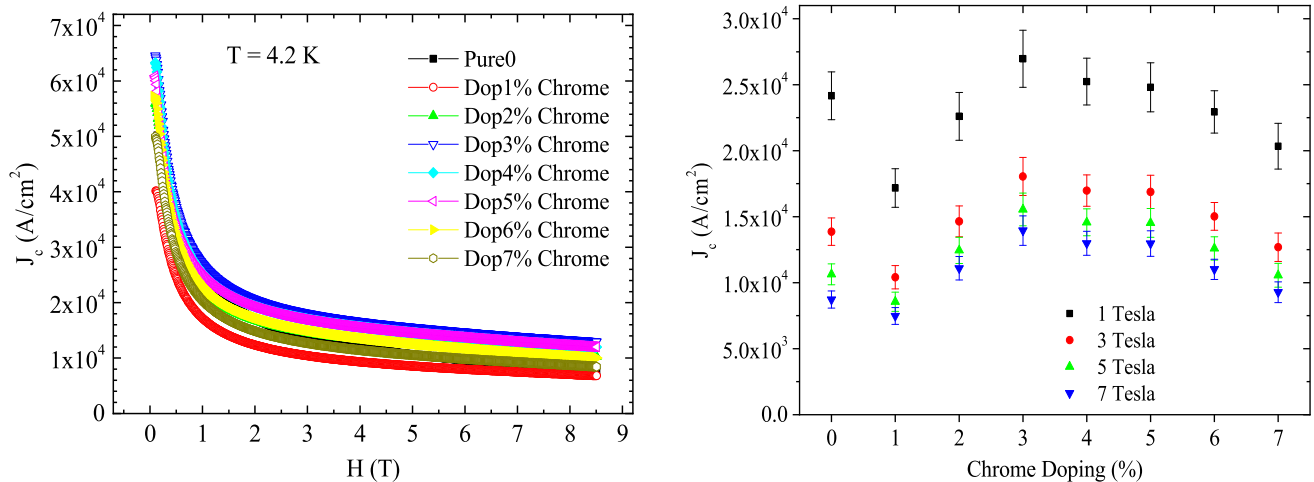


Fig. 6 Critical current density J_c as a function of magnetic field (left) extracted from the $m(H)$ curves in Fig. 5. In the right panel the superconducting critical current for different magnetic fields is plotted as a function of the Chrome doping

This result shows that the presence of Cr inhibits the formation of the Bi2212 phase while increasing the presence of the Bi-2201 secondary phase. Except for a slight effect on grain size, the SEM analysis revealed that the Cr doping has little effect on the surface morphology of the sample.

Studies of DC electrical resistivity versus temperature revealed that Cr doping altered both $T_{c,on}$ and $T_{c,off}$ of the samples.

The Cr6% and Cr2% have the highest values for $T_{c,on}$ and $T_{c,off}$, respectively.

The critical temperature T_c and critical current density J_c as a function of doping concentration were calculated using dc magnetic measurements.

The highest value for T_c was obtained for the Cr4% doped sample due to a possible increase in carrier density with doping.

We also discovered that an initial Cr addition (up to 3%) can provide new favorable pinning centers, improving the pinning landscape of the samples and leading to an increase in J_c .

By continuing to add Cr% to the compound, however, the J_c begins to decrease, most likely due to an excess of impurities, which worsens the compounds' superconductivity phase.

Acknowledgements

The authors gratefully would like to thank Dr. Sevgi Polat Altintas, Pr. Cabir Terzioglu (Abant Izzet Baysal

university, Bolu-Turkey), Pr. Massimiliano Polichetti and Dr. Armando Galluzzi (Salerno university- Italy) for their invaluable supports.

Author contributions

SPA and CT analyzed the XRD, SEM and resistivity results. AG and MP contributed to the magnetic analysis. YB commented on The first draft of the manuscript.

Funding

The authors of this publication note that they were not provided with any funding, grants, or other support during its realization.

Data availability

The authors can be reached for a simple suggestion on the datasets produced and/or examined since the current work.

Declarations

Conflict of interest The authors have no financial statement or other interests to declare.

References

1. R. Foltyn, L. Civale, J.L. MacManus-Driscoll, Q.X. Jia, B. Maiorov, H. Wang, M. Maley, Materials science challenges for high-temperature superconducting wire. *Nat. Mater.* **6**, 631–642 (2007)
2. W.H. Fietz, C. Barth, S. Drotziger, W. Goldacker, R. Heller, S.I. Schlachter, K.P. Weiss, prospects of high temperature superconductors for fusion magnets and power applications. *Fusion Eng. Des.* **88**(6–8), 440–445 (2013)
3. J.G. Bednorz, K.A. Müller, Possible high T_c superconductivity in the Ba-La-Cu-O system. *Zeitschrift für Phys. B Condens. Matter.* **64**, 189–193 (1986). <https://doi.org/10.1007/BF01303701>
4. B. Seeber, *Handbook of Applied Superconductivity* (IOP Publishing Ltd, Bristol, 1998)
5. M. Noe, K.P. Juengst, F.N. Werfel, S. Elschner, J. Bock, F. Breuer, R. Kreutz, Testing bulk HTS modules for resistive superconducting fault current limiters. *IEEE Trans. Appl. Supercond.* **13**, 1976–1979 (2003). <https://doi.org/10.1109/TASC.2003.812953>
6. S. Marinell, D. Bourgault, O. Belmont, A. Sotelo, G. Desgardin, Microstructure and transport properties of YBCO zone melted samples processed in a microwave cavity and infra-red furnace. *Phys. C Supercond. its Appl.* **315**, 205–214 (1999). [https://doi.org/10.1016/S0921-4534\(99\)00202-6](https://doi.org/10.1016/S0921-4534(99)00202-6)
7. F. Ben Azzouz, A. M'Chirgui, B. Yangui, C. Boulesteix, M. Ben Salem, Synthesis, microstructural evolution and the role of substantial addition of PbO during the final processing of (Bi, Pb)-2223 superconductors. *Phys. C Supercond. its Appl.* **356**, 83–96 (2001). [https://doi.org/10.1016/S0921-4534\(01\)0124-1](https://doi.org/10.1016/S0921-4534(01)0124-1)
8. N. Musolino, S. Bals, G. Van Tendeloo, N. Clayton, E. Walker, R. Flükiger, Modulation-free phase in heavily Pb-doped (Bi, Pb)2212 crystals. *Phys. C Supercond. its Appl.* **399**, 1–7 (2003). [https://doi.org/10.1016/S0921-4534\(03\)01324-8](https://doi.org/10.1016/S0921-4534(03)01324-8)
9. Y. Li, S. Kaviraj, A. Berenov, G.K. Perkins, J. Driscoll, A.D. Caplin, G.H. Cao, Q.Z. Ma, B. Wang, L. Wei, Z.X. Zhao, Enhancement of critical current density of (Pb, Sn)-doped Bi-2212 superconductors at high temperature. *Phys. C Supercond. its Appl.* **355**, 51–58 (2001). [https://doi.org/10.1016/S0921-4534\(00\)01770-6](https://doi.org/10.1016/S0921-4534(00)01770-6)
10. P.M. Sarun, S. Vinu, R. Shabna, A. Biju, U. Syamaprasad, Highly enhanced superconducting properties of Eu-doped (Bi, Pb)-2212. *Mater. Lett.* **62**, 2725–2728 (2008). <https://doi.org/10.1016/j.matlet.2008.01.026>
11. S. Vinu, P.M. Sarun, R. Shabna, A. Biju, U. Syamaprasad, Microstructure and transport properties of Bi_{1.6}Pb_{0.5}Sr_{2-x}LuxCa_{1.1}Cu_{2.1}O_{8+δ} superconductor. *Mater. Chem. Phys.* **119**, 135–139 (2010). <https://doi.org/10.1016/j.matchemphys.2009.08.049>
12. S. Uthayakumar, E. Srinivasan, R. Jayavel, C. Subramanian, Substitutional effect of Mn on floating zone growth Bi-2212 bulk textured crystals. *Phys. C Supercond. its Appl.* **383**, 122–126 (2002). [https://doi.org/10.1016/S0921-4534\(02\)01264-9](https://doi.org/10.1016/S0921-4534(02)01264-9)
13. S. Bal, M. Dogruer, G. Yildirim, A. Varilci, C. Terzioglu, Y. Zalaoglu, Role of cerium addition on structural and superconducting properties of Bi-2212 system. *J. Supercond. Nov. Magn.* **25**, 847–856 (2012). <https://doi.org/10.1007/s10948-011-1360-9>
14. O. Ozturk, E. Asikuzun, G. Yildirim, The role of Lu doping on microstructural and superconducting properties of Bi₂Sr₂Ca₁LuxCu₂O_y superconducting system. *J. Mater. Sci. Mater. Electron.* **24**, 1274–1281 (2013). <https://doi.org/10.1007/s10854-012-0918-z>
15. K. Belala, A. Galluzzi, M.F. Mosbah, M. Polichetti, Transport and magnetic properties of Bi(Pb)2212 superconducting ceramics doped by low rate of potassium. *Mater. Sci.* **39**, 15–23 (2021). <https://doi.org/10.2478/msp-2021-0005>
16. O. Ozturk, E. Asikuzun, M. Coskunyurek, N. Soyulu, A. Hancerliogullari, A. Varilci, C. Terzioglu, The effect of Nd₂O₃ addition on superconducting and structural properties and activation energy calculation of Bi-2212 superconducting system. *J. Mater. Sci. Mater. Electron.* **25**, 444–453 (2014). <https://doi.org/10.1007/s10854-013-1608-1>
17. E. Asikuzun, O. Ozturk, H.A. Cetinkara, G. Yildirim, A. Varilci, M. Yilmazlar, C. Terzioglu, Vickers hardness measurements and some physical properties of Pr₂O₃ doped Bi-2212 superconductors. *J. Mater. Sci. Mater. Electron.* **23**, 1001–1010 (2012). <https://doi.org/10.1007/s10854-011-0537-0>
18. S. Menassel, M.F. Mosbah, Y. Boudjadja, S.P. Altintas, A. Varilci, C. Terzioglu, Effect Y substitution on the microstructure, transport and magnetic properties of Bi₂Sr₂Ca₁Cu₂O_{8+δ} superconducting ceramics. *Mater. Sci. Pol.* **34**, 582–590 (2016). <https://doi.org/10.1515/msp-2016-0077>
19. I. Chong, Z. Hiroi, M. Izumi, J. Shimoyama, Y. Nakayama, K. Kishio, T. Terashima, Y. Bando, M. Takano, High critical-current density in the heavily Pb-doped Bi₂Sr₂CaCu₂O_{8+δ} superconductor: Generation of efficient pinning centers. *Science* (80-.) **276**, 770–773 (1997). <https://doi.org/10.1126/science.276.5313.770>
20. R. Funahashi, I. Matsubara, K. Ueno, K. Mizuno, Isotropic pinning in heavily Pb-doped Bi-2212/Ag tapes. *Phys. C Supercond. its Appl.* **315**, 247–253 (1999). [https://doi.org/10.1016/S0921-4534\(99\)00237-3](https://doi.org/10.1016/S0921-4534(99)00237-3)

21. L. Shi, Q. Dong, Y. Zhang, Effect of Pb-doping and annealing on the structure and T_c of Bi-2212 phase superconductor. *Phys. C Supercond. its Appl.* **341–348**, 649–650 (2000). [https://doi.org/10.1016/S0921-4534\(00\)00632-8](https://doi.org/10.1016/S0921-4534(00)00632-8)
22. D.M. Pooke, G.V.M. Williams, Oxygen loading in (Bi, Pb)-2212 and -2223 materials. *Phys. C Supercond. its Appl.* **354**, 396–400 (2001). [https://doi.org/10.1016/S0921-4534\(01\)00107-1](https://doi.org/10.1016/S0921-4534(01)00107-1)
23. F. Jean, G. Collin, M. Andrieux, N. Blanchard, A. Forget, S. Rousseau, J.F. Marucco, Oxygen excess in Bi-2212: study of a Pb-substituted compound. *Phys. C Supercond. its Appl.* **384**, 345–350 (2003). [https://doi.org/10.1016/S0921-4534\(02\)01969-X](https://doi.org/10.1016/S0921-4534(02)01969-X)
24. Raheleh Yousefi Seyede, Sobhani Azam, Salavati-Niasari. Masoud, A new nanocomposite superionic system (CdHgI₄/HgI₂): Synthesis, characterization and experimental investigation. *Adv. Powder Technol.* **28**, 1258–1262 (2017). <https://doi.org/10.1016/j.apt.2017.02.013>
25. M.R. Presland, J.L. Tallon, R.G. Buckley, R.S. Liu, N.E. Flower, General trends in oxygen stoichiometry effects on T_c in Bi and Tl superconductors. *Phys. C Supercond. its Appl.* **176**, 95–105 (1991). [https://doi.org/10.1016/0921-4534\(91\)90700-9](https://doi.org/10.1016/0921-4534(91)90700-9)
26. H.R. Zhuang, H. Kozuka, S. Sakka, Preparation of superconducting Bi-Sr-Ca-Cu-O ceramics by the sol-gel method. *J. Mater. Sci.* **25**, 4762–4766 (1990). <https://doi.org/10.1007/BF01129938>
27. N. Hara, R. Ogawa, Y. Kawate, T. Tateishi, Preparation of Bi based high-T_c superconductors containing Pb and Sb by the sol-gel method. *J. Mater. Res.* **7**, 292–298 (1992). <https://doi.org/10.1557/JMR.1992.0292>
28. K. Ma, A.C. Pierre, Sol-gel processing of high-T_c superconductors in the Bi-(Pb)-Sr-Ca-Cu-O system. *J. Mater. Res.* **7**, 1328–1335 (1992). <https://doi.org/10.1557/JMR.1992.1328>
29. B.S. Ahn, Synthesis of BiSrCaCu(Ni)O ceramics from the gel precursors and the effect of Ni substitution. *Bull. Korean Chem. Soc.* **23**, 1304–1308 (2002). <https://doi.org/10.5012/bkcs.2002.23.9.1304>
30. F.H. Chen, H.S. Koo, T.Y. Tseng, Synthesis of high-T_c superconducting Bi-Pb Sr-Ca-Cu-O ceramics prepared by an ultrastructure processing via the oxalate route. *J. Mater. Sci.* **25**, 3338–3346 (1990). <https://doi.org/10.1007/BF00587696>
31. T.S. Hen, J.R. Chen, T.Y. Tseng, Preparation of Bi_{0.7}Pb_{0.3}Sr_{1.0}Ca_{1.0}Cu_{1.8}O_y high-tc superconductor by the citrate method. *Jpn. J. Appl. Phys.* **29**, 652–655 (1990). <https://doi.org/10.1143/JJAP.29.652>
32. T.M. Chen, Y.H. Hu, Polymeric precursors for the preparation of Bi_{1.5}Pb_{0.5}Sr₂Ca₂Cu₃O_x. *J. Solid State Chem.* **97**, 124–130 (1992). [https://doi.org/10.1016/0022-4596\(92\)90016-0](https://doi.org/10.1016/0022-4596(92)90016-0)
33. Raheleh Yousefi Seyede, Abbas Alshamsi Hassan, Omid Amiri, Salavati-Niasari. Masoud, Synthesis, characterization and application of Co/Co₃O₄ nanocomposites as an effective photocatalyst for discoloration of organic dye contaminants in wastewater and antibacterial properties. *J. Mol. Liq.* **337**, 116405 (2021). <https://doi.org/10.1016/j.molliq.2021.116405>
34. A. Galluzzi, K. Buchkov, E. Nazarova, V. Tomov, G. Grimaldi, A. Leo, S. Pace, M. Polichetti, Transport properties and high upper critical field of a Fe(Se, Te) iron based superconductor. *Eur. Phys. J. Spec. Top.* (2019). <https://doi.org/10.1140/epjst/e2019-800169-5>
35. A. Galluzzi, K.M. Buchkov, E. Nazarova, V. Tomov, G. Grimaldi, A. Leo, S. Pace, M. Polichetti, Pinning energy and anisotropy properties of a Fe(Se, Te) iron based superconductor. *Nanotechnology.* **30**, 254001 (2019). <https://doi.org/10.1088/1361-6528/ab0c23>
36. A. Galluzzi, D. Mancusi, C. Cirillo, C. Attanasio, S. Pace, M. Polichetti, Determination of the transition temperature of a weak ferromagnetic thin film by means of an evolution of the method based on the Arrott Plots. *J. Supercond. Nov. Magn.* **31**, 1127–1132 (2018). <https://doi.org/10.1007/s10948-017-4281-4>
37. A. Galluzzi, A. Nigro, R. Fittipaldi, A. Guarino, S. Pace, M. Polichetti, DC magnetic characterization and pinning analysis on Nd_{1.85}Ce_{0.15}Cu₄O₄ cuprate superconductor. *J. Magn. Magn. Mater.* **475**, 125–129 (2019). <https://doi.org/10.1016/J.JMMM.2018.11.119>
38. Galluzzi, A., Buchkov, K., Tomov, V., Nazarova, E., Leo, A., Grimaldi, G., Nigro, A., Pace, S., Polichetti, M.: Second Magnetization Peak Effect in a Fe(Se,Te) iron based superconductor. In: *Journal of Physics: Conference Series*. p. 012012. IOP Publishing (2019)
39. M. Polichetti, A. Galluzzi, K. Buchkov, V. Tomov, E. Nazarova, A. Leo, G. Grimaldi, S. Pace, A precursor mechanism triggering the second magnetization peak phenomenon in superconducting materials. *Sci. Rep.* **11**, 7247 (2021). <https://doi.org/10.1038/s41598-021-86728-8>
40. V. Petricek, M. Dušek, L. Palatinus, Crystallographic computing system JANA2006: general features. *Zeitschrift für Krist.* **229**, 345–352 (2014). <https://doi.org/10.1515/zkri-2014-1737>
41. A. Amira, Y. Boudjadja, A. Saouadel, A. Varilci, M. Akdogan, C. Terzioglu, M.F. Mosbah, Effect of doping by low content of yttrium at Ca and Sr sites of Bi(Pb)-2212 superconducting ceramics. *Phys. B Condens. Matter.* **406**, 1022–1027 (2011). <https://doi.org/10.1016/j.physb.2010.12.052>
42. H.M. Rietveld, *J. Appl. Cryst.* **2**(2), 65–71 (1969)
43. A. Naseem, Shakeel, Khan, Effect of (Mn-Co) co-doping on the structural, morphological, optical, photoluminescence and

- electrical properties of SnO₂. *J. Alloy. Compd.* **720**, 502–509 (2017). <https://doi.org/10.1016/j.jallcom.2017.05.293>
44. A. Naseem, Shakeel, Khan, Mohd, Mohsin Nizam Ansari, Optical, dielectric and magnetic properties of Mn doped SnO₂ diluted magnetic semiconductors. *Ceram. Int.* **44**, 15972–15980 (2018). <https://doi.org/10.1016/j.ceramint.2018.06.024>
 45. B. Jayaram, P.C. Lanchester, M.T. Weller, Localization and interaction effects during superconductor-insulator transition of Bi₂Sr₂Ca_{1-x}Gd_xCu₂O_{8+d}. *Phys. Rev. B.* **43**, 5444–5450 (1991). <https://doi.org/10.1103/PhysRevB.43.5444>
 46. B.D. Cullity, *Element of X-ray diffraction* (Addison-Wesley, Boston, 1978)
 47. Y. Boudjadja, A. Amira, N. Mahamdioua, A. Saouadel, S. Menassel, A. Varilci, C. Terzioglu, S.P. Altintas, Microstructural and magneto-transport properties of Bi_{1.6}Pb_{0.4}Sr₂Ca_{1-x}Gd_xCu₂O_{8+δ} superconducting ceramics. *Phys. B Condens. Matter.* **505**, 68–73 (2017). <https://doi.org/10.1016/j.physb.2016.10.035>
 48. C. Böhmer et al., *Supercond. Sci. Technol.* **10** (1997). [Y. Enomoto et al. *J. Phys. Condens. Matter* **9** (1997)].
 49. O. Kraut, C. Meingast, G. Bräuchle, H. Claus, A. Erb, G. Müller-Vogt, H. Wühl, Uniaxial pressure dependence of T_c of untwinned YBa₂Cu₃O_x single crystals for x=6.5–7. *Phys. C Supercond. its Appl.* **205**, 139–146 (1993). [https://doi.org/10.1016/0921-4534\(93\)90180-X](https://doi.org/10.1016/0921-4534(93)90180-X)
 50. H. Claus, M. Braun, A. Erb, K. Röhberg, B. Runtsch, H. Wühl, G. Bräuchle, P. Schweib, G. Müller-Vogt, Löhneysen, H. v.: The “90 K” plateau of oxygen deficient YBa₂Cu₃O_{7-δ} single crystals. *Phys. C Supercond. Appl.* **198**, 42–46 (1992). [https://doi.org/10.1016/0921-4534\(92\)90263-C](https://doi.org/10.1016/0921-4534(92)90263-C)
 51. D. Dew-Hughes, Flux pinning mechanisms in type II superconductors. *Philos. Mag.* **30**, 293–305 (1974). <https://doi.org/10.1080/14786439808206556>
 52. L. Zhang, Q. Qiao, X.B. Xu, Y.L. Jiao, L. Xiao, S.Y. Ding, X.L. Wang, Surface barrier and bulk pinning in MTG YBa-CuO. *Phys. C Supercond. its Appl.* **445–448**, 236–239 (2006). <https://doi.org/10.1016/j.physc.2006.04.008>
 53. C.P. Bean, Magnetization of hard superconductors. *Phys. Rev. Lett.* **8**, 250–253 (1962). <https://doi.org/10.1103/PhysRevLett.8.250>
 54. C.P. Bean, Magnetization of high-field superconductors. *Rev. Mod. Phys.* **36**, 31–39 (1964). <https://doi.org/10.1103/RevModPhys.36.31>
 55. A. Umezawa, G.-W. Crabtree, J.-Z. Liu, H.-W. Weber, W.-K. Kwok, L.-H. Nurez, T.J. Morun, C.-H. Sowers, H. Claus, Enhanced critical magnetization currents due to fast neutron irradiation in single-crystal YBa₂Cu₃O_{7+δ}. *Phys. Rev. B* **36**, 7151–7153 (1987)
 56. W. Zhou, X. Xing, W. Wu, H. Zhao, Z. Shi, Second magnetization peak effect, vortex dynamics, and flux pinning in 112-type superconductor Ca_{0.8}La_{0.2}Fe_{1-x}CoxAs₂. *Sci. Rep.* **6**, 22278 (2016). <https://doi.org/10.1038/srep22278>
 57. A. Galluzzi, K. Buchkov, V. Tomov, E. Nazarova, A. Leo, G. Grimaldi, A. Nigro, S. Pace, M. Polichetti, Evidence of pinning crossover and the role of twin boundaries in the peak effect in FeSeTe iron based superconductor. *Supercond. Sci. Technol.* **31**, 015014 (2018). <https://doi.org/10.1088/1361-6668/aa9802>
 58. Miu, L., Ionescu, A.M., Miu, D., Ivan, I., Crisan, A.: Behavior of the Second Magnetization Peak in Self-nanostructured La_{2-x}Sr_xCuO₄ Single Crystals. Presented at the (2017)
 59. A. Galluzzi, M. Polichetti, K. Buchkov, E. Nazarova, D. Mancusi, S. Pace, Evaluation of the intragrain critical current density in a multidomain FeSe crystal by means of dc magnetic measurements. *Supercond. Sci. Technol.* **28**, 115005 (2015). <https://doi.org/10.1088/0953-2048/28/11/115005>
 60. M.G. Adesso, C. Senatore, M. Polichetti, S. Pace, Harmonics of the AC susceptibility as probes to differentiate the various creep models. *Phys. C Supercond.* **404**, 289–292 (2004). <https://doi.org/10.1016/j.physc.2003.09.096>
 61. M.G. Adesso, M. Polichetti, S. Pace, Harmonics of the AC susceptibility for the study of I-V curves in melt grown YBCO. *Phys. C Supercond. Appl.* **401**, 196–200 (2004). <https://doi.org/10.1016/j.physc.2003.09.036>
 62. C. Senatore, M. Polichetti, D. Zola, T.D. Matteo, G. Giunchi, S. Pace, Vortex dynamics and pinning properties analysis of MgB₂ bulk samples by ac susceptibility measurements. *Supercond. Sci. Technol.* **16**, 183–187 (2003). <https://doi.org/10.1088/0953-2048/16/2/310>

Publisher's Note Springer Nature remains neutral with regard to jurisdictional claims in published maps and institutional affiliations.

Springer Nature or its licensor (e.g. a society or other partner) holds exclusive rights to this article under a publishing agreement with the author(s) or other rightsholder(s); author self-archiving of the accepted manuscript version of this article is solely governed by the terms of such publishing agreement and applicable law.